Proc. Natl. Acad. Sci. USA
Vol. 92, pp. 8185–8189, August 1995
Developmental Biology

Cryptorchidism and homeotic transformations of spinal nerves and vertebrae in *Hoxa-10* mutant mice

(*Hox* genes/segmentation/positional information/fertility)

FILIPPO M. RIJLI†, ROBERT MATYAS†, MASSIMO PELLEGRINI‡, ANDRÉE DIERICH†, PETER GRUSS‡, PASCAL DOLLÉ†, AND PIERRE CHAMBON†§

†Institut de Génétique et de Biologie Moleculaire et Cellulaire, Centre National de la Recherche Scientifique/Institut National de la Santé et de la Recherche Médicale/Université Louis Pasteur, Collège de France, BP 163, 67404 Illkirch-Cedex, France; and ‡Department of Molecular Cell Biology, Max Planck Institute of Biophysical Chemistry, Am Fassberg, 37077 Göttingen, Germany

Contributed by Pierre Chambon, June 2, 1995

ABSTRACT **Homozygous mice mutated by homologous recombination for the *AbdB*-related *Hoxa-10* gene are viable but display homeotic transformations of vertebrae and lumbar spinal nerves. Mutant males exhibit unilateral or bilateral criptorchidism due to developmental abnormalities of the gubernaculum, resulting in abnormal spermatogenesis and sterility. These results reveal an important role of *Hoxa-10* in patterning posterior body regions and suggest that *Hox* genes are involved in specifying regional identity of both segmented and nonovertly segmented structures of the developing body.**

Gene knock-outs in mice led to the conclusion that *Hox* genes, which are evolutionarily related to the *Drosophila* homeotic genes, play a key role in the morphogenesis of segmented structures along the primary body axis, such as branchial arches, vertebrae, cranial nerves, and ganglia (1). However, little is still known about *Hox* gene function in patterning of nonovertly segmented structures, such as the spinal cord and the internal organs. The 5′-located genes of the four vertebrate *Hox* complexes are related to the *AbdB* gene, which specifies the identity of the *Drosophila* posterior segments. *AbdB*-related *Hox* genes are sequentially activated in the most posterior part of the mouse embryo (2). For instance, the *AbdB*-related *Hoxa-10* gene is expressed in somite derivatives, with an expression boundary in prevertebrae 20 and 21, the spinal cord, posterior abdominal regions, the genital tubercle, and the limbs (3). Gene knock-out by homologous recombination was used here to demonstrate that the *Hoxa-10* gene plays an important role in patterning several segmented and nonsegmented structures of the posterior region of the mouse body.

MATERIALS AND METHODS

Mouse lines bearing a disrupted *Hoxa-10* gene were obtained as follows: 11-kb *Kpn* I and 5.4-kb *Bam*HI genomic fragments containing the *Hoxa-10* gene were subcloned from COS4H2 into pBC (Stratagene) and into pSPT18 to yield MP1 and MP2, respectively. A *neo* (neomycin resistance) gene (containing a polyadenylylation signal) driven by a phosphoglycerate kinase (PGK) gene promoter (4) was inserted, in the same transcriptional orientation of *Hoxa-10*, into the *Xho* I site of the homeobox in MP2, thus yielding MP5. A *Sal* I–*Nhe* I 5.8-kb fragment of MP5 (containing *Hoxa-10* genomic sequences plus the *neo* cassette) was subcloned into a pBS (Stratagene) vector containing a thymidine kinase (TK) cassette in the polylinker, and a *Sal* I–*Sal* I 6.7-kb fragment from MP1 was subcloned into this plasmid, thus generating the targeting construct MP9. Embryonic stem (ES) cell culture, homologous recombination, DNA extraction, and Southern blot analysis were as described (5). The probe used for homologous recombination screening was a MP1 1.2-kb *Nhe* I–*Kpn* I genomic fragment 3′-external to the targeting construct. This probe recognized a 3.0-kb *Eco*RI fragment in the wild-type (wt) allele and a 4.8-kb fragment in the mutated allele. Upon electroporation of 10^7 D3 ES cells, 3 targeted ES cell clones were obtained by using described procedures (5). Two of these clones yielded two lines of *Hoxa-10* mutant mice with indistinguishable phenotypes. The effect of the mutation was studied both in inbred (129Sv) and mixed (129Sv/C57BL/6) genetic backgrounds.

Alcian blue/alizarin red skeletal stainings were as described (5). For macroscopic examination and histology, organs were dissected and fixed in formalin or Bouin solution for several days. Alternatively, animals were perfused with 4% paraformaldehyde. *In situ* hybridization was as described (2).

RESULTS

Hoxa-10$^{+/-}$ mutants were viable and fertile. Homozygous mutants were viable and had a normal lifetime span, but their fertility was impaired.

Cryptorchidism in *Hoxa-10* Mutants. Of six *Hoxa-10*$^{-/-}$ females bred to fertile males, only three gave birth to small litters over a 5-week breeding period. No macroscopic abnormalities were observed upon dissection of the genital tract and internal organs of mutant females (not shown). However, histological analysis revealed numerous endometrial cysts in the uteri of 8 of 10 mutant females (not shown), which might account for their reduced fertility. *Hoxa-10*$^{-/-}$ males were sterile or markedly hypofertile. External examination of 14 *Hoxa-10*$^{-/-}$ males with a mixed (129Sv/C57BL/6) genetic background revealed a high incidence of cryptorchid testes either unilaterally (8 of 14; in all cases, the left testis was undescended) or bilaterally (6 of 14, with no scrotal sac and reduced ano–genital distance). Interestingly, all of the five examined mutants with 129Sv inbred background had bilateral cryptorchidism. Fig. 1*A* shows the dissected abdominal region of an adult homozygous mutant with bilateral intraabdominal testes. Testes were usually located near the bladder (not shown).

The descent of the testes from midthoracic to abdominal positions during fetal life and through the inguinal canal into the scrotal sac after birth (in the mouse) has been proposed to depend on dynamic morphological changes of a ligamentous cord called gubernaculum, which connects the gonad to the labioscrotal swellings of the abdominal wall (6). The inguinal canal and scrotal sac are formed following outgrowth of the peritoneum (vaginal process) and eversion of the cremaster

The publication costs of this article were defrayed in part by page charge payment. This article must therefore be hereby marked "*advertisement*" in accordance with 18 U.S.C. §1734 solely to indicate this fact.

Abbreviations: wt, wild type; dpc, days postcoitum; STN, supernumerary intercostal nerve; GFN, genitofemoral nerve.

§To whom reprint requests should be addressed.

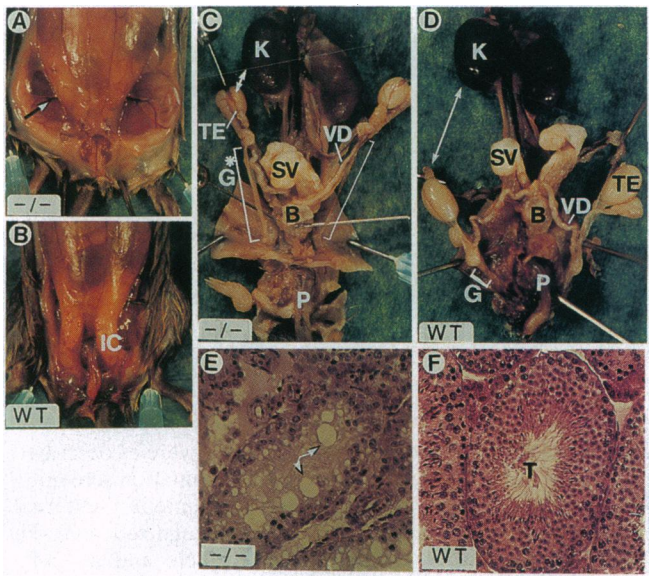

FIG. 1. Criptorchidism in *Hoxa-10*$^{-/-}$ adult males. (*A* and *B*) Dissected abdominal regions of an adult homozygous mutant (*A*) and wt (*B*) mouse (129Sv inbred). The mutant (−/−) lacks the inguinal canals (IC in *B*), and both testes have an intraabdominal location (the arrow in *A* indicates the position of one testis beneath the peritoneum). (*C* and *D*) Dissected genitalia of the mice shown in *A* and *B*. In wt adult mice (*D*), the gubernaculum (G) is a short remnant anchoring the testis to the skin of the scrotal sac, whereas it is present bilaterally in the mutant (*C*) as a long cord connecting the testis to the abdominal wall (G*). No formation of inguinal canal and/or scrotal sac is visible at the site of attachment of the gubernaculum on the abdominal wall. Note that the size of the testes is reduced in the mutant. (*E* and *F*) Histology of a criptorchid testis from a mutant adult male (*E*) and a descended testis from an adult wt male (*F*). Mature sperm cells are visible in wt seminiferous tubule lumen but not in mutant testis. Sloughing of germ cells at various stages of maturation and vacuolization of Sertoli cells (arrows) are visible in *E*. Seminiferous tubules of mutant and wt prenatal testes were indistinguishable (18.5 dpc fetuses; not shown), indicating that the lesions at the adult stage were secondary to cryptorchidism. IC, inguinal canal; K, kidney; SV, seminal vesicle; TE, testis; VD, vas deferens; B, bladder; P, penis; G, gubernaculum; T, seminiferous tubule.

muscle. Careful dissection revealed a specific abnormality of the gubernaculum in *Hoxa-10*$^{-/-}$ adult mutant males (Fig. 1*C*). Histological analysis of *Hoxa-10*$^{-/-}$ fetuses 18.5 days postcoitum (18.5 dpc) confirmed that the gubernaculum did not undergo normal morphological changes at its distal end (gubernacular bulb), nor did it foreshorten as in wt controls (not shown). Furthermore, the vaginal process, the inguinal canal, and the scrotal sac were either missing or partially formed (not shown). The size of the testes of *Hoxa-10*$^{-/-}$ adult mutants was reduced (compare Fig. 1 *C* and *D*). Histology of adult criptorchid testes revealed marked lesions of the seminiferous tubules, with blocks of spermatogenesis, sloughing of germ cells at various stages of maturation, and vacuolization of Sertoli cells (compare Fig. 1 *E* and *F*). All of these defects likely correspond to a functional degeneration secondary to the persistent intraabdominal location of the testes (ref. 7 and references therein) and explain the infertility of male *Hoxa-10*$^{-/-}$ mutants.

Axial Skeleton Homeosis and Rib Alterations. The vertebral pattern was altered in adult *Hoxa-10*$^{-/-}$ mutant skeletons with both incomplete penetrance and variable expressivity, depending on the genetic background (not shown). The presence of a supernumerary pair of ribs on the 21st vertebra (in 28 of 30 mutants) was interpreted as an anterior homeotic transformation of L1 toward a thoracic identity (Fig. 2*B*). The next *Hoxa-10*$^{-/-}$ lumbar vertebrae also showed partial anterior transformations (Fig. 2*D*; see the legend for details). The *Hoxa-10*$^{-/-}$ sacral vertebrae were usually unaffected, except in 3 mutants of 30 in which S1 and S2 were asymmetrically transformed. In these cases, the S1 right side was correctly articulated with the right ilium bone, whereas the S1 left side harbored L6-like transverse processes, the left ilium bone thus articulating to S2 (not shown). Only 1 mutant of 30 displayed a full transformation of S1/S2 (not shown).

In 9 of 30 *Hoxa-10*$^{-/-}$ mutants, only six pairs of ribs contacted the sternum instead of seven in wt (Fig. 2 *E* and *F*). Furthermore, each mutant rib from the 7th to the 12th (9 of 30 mutants), from the 9th to the 12th (6 of 30), and from the 10th to the 12th (15 of 30) was shortened and displayed features resembling the next caudal wt rib rather than its corresponding wt counterpart (Fig. 2 *G–J*, and data not shown). The 10th thoracic vertebra (T10) is the most caudal vertebra to display typical thoracic features in wt mice (8). In *Hoxa-10*$^{-/-}$ mutants, T10 displayed "lumbar-type" features, thus resembling wt T11, whereas T9 appeared to have features of wt T10 (15 of 30 mutants) (not shown). Thus, morphology of both ribs and vertebrae suggest that the T6–T12 region of *Hoxa-10*$^{-/-}$ mutants has been partially transformed posteriorly by one segment. The T13 vertebra represents a "neutral" segment between the posteriorly transformed (thoracic) and anteriorly transformed (lumbar) regions. *Hoxa-10*$^{+/-}$ mutants usually displayed similar, though milder alterations than those seen in homozygous mutants (not shown).

Neighbor *Hox* Gene Expression Domains Are Not Altered in *Hoxa-10*$^{-/-}$ Mice. No alteration of the distribution of *Hoxa-9* transcript domains could be detected by *in situ* hybridization in 12.5-dpc *Hoxa-10*$^{-/-}$ (Fig. 3*B*) or *Hoxa-10*$^{+/-}$ mutant embryos (not shown). The distribution of *Hoxa-11* transcripts was also normal in *Hoxa-10*$^{-/-}$ or *Hoxa-10*$^{+/-}$ embryos (not shown). A "*neo*" probe was included in this analysis, since it can detect transcripts from the promoter of the disrupted *Hox* gene (5) and from the *neo* promoter itself (9). Interestingly, the *neo* transcript signal extended up to rostral boundaries that did not correspond to the wt *Hoxa-10* expression boundaries (prevertebrae 20 and 21; spinal cord boundary at the level of prevertebrae 16 and 17) but were aligned to those of the *Hoxa-9* gene (prevertebra 13; spinal cord boundary at the level of prevertebra 5) both in homozygous (Fig. 3*B*) and heterozygous mutants (not shown).

Morphological Transformation of Spinal Nerves. Dissected spinal cords of adult wt and *Hoxa-10*$^{-/-}$ mice were aligned at the level of the lumbar region (Fig. 4 *A* and *B*, respectively). In wt, the last thoracic nerve (a in Fig. 4*A*) arises between T13 and L1 and consists of two roots (open double-headed arrow), one of which joins one root of the first lumbar nerve (b). In the mutant (Fig. 4*B*), a nerve with similar morphology and anatomical relationships (a′; double-headed arrow) was found shifted posteriorly by one segment between T13* and L1* (mutant lumbar vertebrae are indicated according to their transformed morphology T13*–L5* corresponding to wt L1–L6, respectively). Instead, a nerve with an intercostal nerve feature is found between T13 and T13* (STN in Fig. 4*B*). STN innervated additional intercostal muscles (Fig. 4*B*, and data not shown), and a supernumerary intercostal artery was present (arrowhead in Fig. 4*B*). Comparison of the branching patterns and anatomical relationships of the next caudal nerves revealed that, in the mutant, each nerve adopted the morphology of its closest rostral wt counterpart (compare Fig. 4 *A* and *B*) so that the nerves between L1* and L2*, L2* and L3*, L3* and L4*, and L4* and L5* corresponded to the wt first to fourth lumbar nerves (see the legend to Fig. 4). There was no nerve morphologically corresponding to the wt fifth lumbar nerve (f in Fig. 4*A*), and the wt sixth lumbar nerve (g between wt L6 and S1) (Fig. 4*A*) appeared unchanged in the mutant between L5* and S1 (Fig. 4*B*). Since the number of presacral nerves was the same in mutant and wt mice, these findings

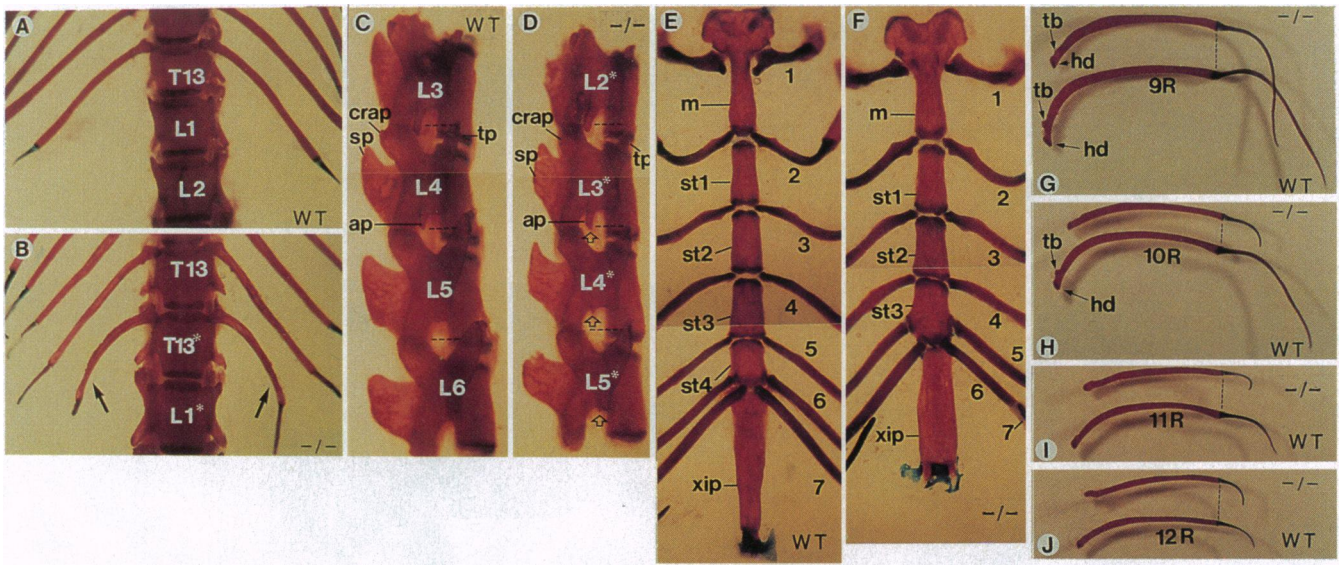

FIG. 2. (*A–D*) Anterior homeosis of lumbar vertebrae. (*A* and *B*) Ventral views of adult T13 to L2 vertebrae and ribs in a wt mouse (*A*) and *Hoxa-10*$^{-/-}$ mutant (−/−) mouse (129Sv inbred) that displays a full extra pair of ribs on L1 (*B*, arrows). (*C* and *D*) Lateral views of the L3–L6 vertebrae of wt (*C*) and *Hoxa-10* mutant (−/−) (*D*) (129Sv inbred). Mutant lumbar vertebrae are indicated according to their transformed morphology T13*–L5* corresponding to wt L1–L6, respectively. Compare each mutant vertebra to its wt counterpart and to the next anterior wt vertebra. wt lumbar vertebrae present bilateral accessory processes that progressively decrease in size from L3 to L5. The accessory processes on L5 are absent or reduced to small tips, whereas L6 has no distinct accessory processes. L3* and L4* have larger accessory processes than their wt counterparts, resembling wt L3 and L4, respectively (open arrows). L5* displays a small tip reminiscent of a wt L5 accessory process (open arrow). L2*–L5* transverse processes are reduced compared with their wt counterparts [compare with the sizes of the cranial articular processes (dashed lines)], making each of them resemble somewhat its next anterior wt neighbor. ap, Accessory process; crap, cranial articular process; sp, spinous process; tp, transverse process. (*E–J*) Posterior homeosis of thoracic vertebrae. (*E* and *F*) Comparison of the thoracic cages and sternum of wt (*E*) and mutant (−/−) (*F*) adult mice (hybrid background). In wt, 7 pairs of ribs contact the sternum. The first 6 ribs are separated by sternebrae (the manubrium sterni S1 and S2–S5), whereas the 6th and 7th ribs articulate to the same sternebra. Only 6 pairs of ribs contact the sternum in the mutant (*F*). The 7th ribs end freely, thus resembling wt 8th ribs. The 5th and 6th pair of mutant ribs contact the same sternebra, and the sternum lacks an entire sternebra. The xiphoid process is also reduced in this mutant. (*G–J*) Comparison of the 9th (*G*) to the 12th (*J*) ribs of a wt and a *Hoxa-10*$^{-/-}$ mutant (hybrid background). The mutant rib (−/−) is above the wt rib. Moving caudally, wt rib size decreases particularly between the 10th and 11th ribs (compare 10R and 11R in *H* and *I*). Ribs until the 10th pair articulate to the vertebrae by their heads and adjacent rib tubercles, whereas 11th and 12th ribs have no well-defined tubercles. The *Hoxa-10*$^{-/-}$ 8th–12th ribs are reduced in size, each resembling the next caudal wt rib rather than its corresponding wt counterpart (*G–J*). Moreover, the *Hoxa-10*$^{-/-}$ 9th and 10th ribs display no well-defined rib tubercles (*G* and *H*), a feature of more caudal wt ribs. hd, Rib head; R, rib; m, manubrium; st, sternebra; tb, rib tubercle; xip, xiphoid process.

suggest that in *Hoxa-10*$^{-/-}$ mutants, each spinal nerve between vertebrae T13 and L5* (corresponding to wt T13–L6) has been homeotically transformed to the closest wt anterior identity, with the last thoracic nerve transformed to an intercostal nerve identity, the first lumbar nerve transformed to a last thoracic nerve identity, and the second to fifth lumbar nerves transformed to first to fourth lumbar nerve identity.

DISCUSSION

In addition to the above abnormalities (see *Results*), the *Hoxa-10*$^{-/-}$ mutants display alterations of the limb proximal skeletal elements that will be described elsewhere.

Hoxa-10$^{-/-}$ males exhibit intraabdominal cryptorchid testes, and this phenotype causes sterility when bilateral. The left testis was always found undescended in homozygotes exhibiting unilateral cryptorchidism, suggesting a nonstochastic expressivity of the mutation. An independent *Hoxa-10* mutation also resulted in mutants with cryptorchid testes and spermatogenesis defects very similar to those described here, even though bilateral cryptorchidism was fully penetrant (10). Analysis of *Hoxa-10*$^{-/-}$ cryptorchid mice revealed abnormalities of the gubernaculum (the gubernacular bulb failed to differentiate), the inguinal canal, and the scrotal sac. *Hoxa-10* is expressed in the gubernaculum from 15.5 dpc onward (10), and is also expressed by 13.5–14.5 dpc along the ventromedial region of the developing abdominal wall (not shown), prior to the morphogenetic events leading to the formation of the inguinal canal and scrotal sac. Whether the labeled cell layers corresponded to abdominal muscle precursors (from which the

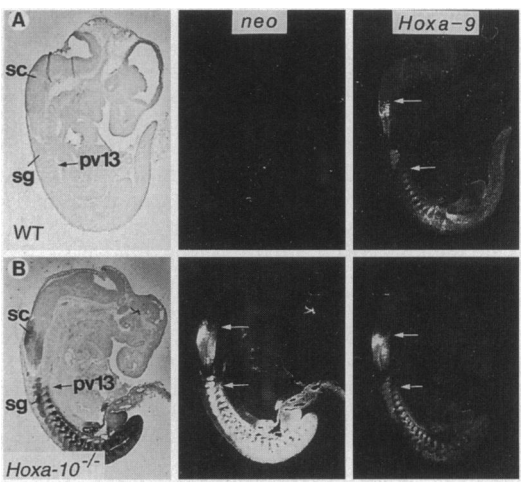

FIG. 3. *In situ* hybridization analysis of *Hoxa-9* and *neo* transcripts in wt (*A*) and *Hoxa-10*$^{-/-}$ (*B*) 12.5-dpc embryos. Adjacent sagittal sections of a wt (*A*) and *Hoxa-10*$^{-/-}$ (*B*) 12.5-dpc embryos hybridized to *neo* and *Hoxa-9* probes. (*Left*) Bright-field views. The *Hoxa-9* prevertebral transcript boundary in *Hoxa-10*$^{-/-}$ mutant is the same as in wt (white arrows), starting in pv 13 (T6), but with higher signal intensities in the thoracic pv and rib anlagen. The *Hoxa-9* transcript boundaries in the spinal cord and ganglia (at the level of prevertebra 5) are also unaltered in mutant embryos (white arrows). Note that in *Hoxa-10*$^{-/-}$ mutant (*B*), the *neo* and *Hoxa-9* transcript domains and boundaries are very similar (white arrows). The *neo* signal is however stronger (visible in black on the bright-field views) and does not gradually decrease, as the *Hoxa-9* signal does in posterior regions of the embryo. pv, Prevertebra; sc, spinal cord; sg, spinal ganglion.

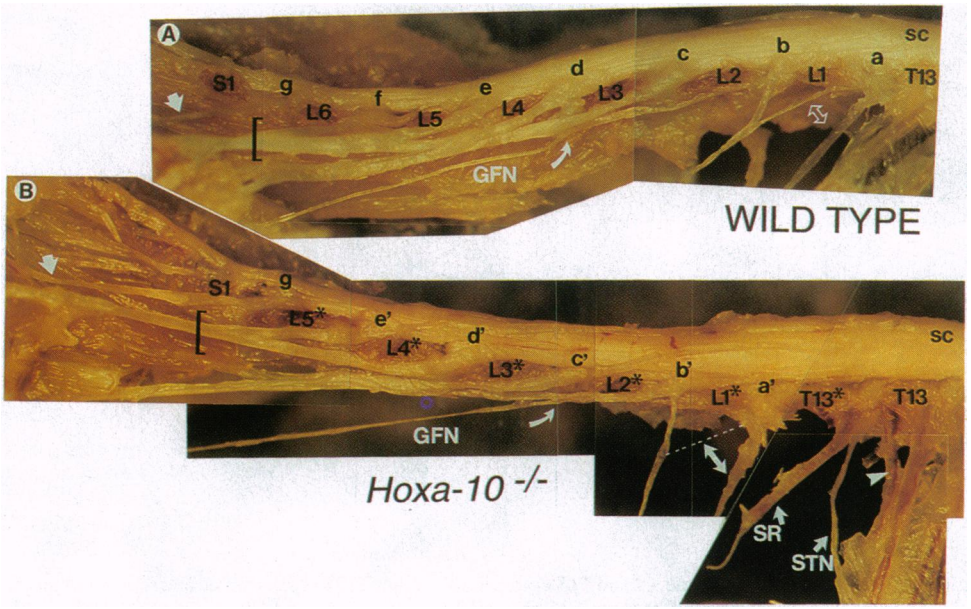

FIG. 4. Transformation of the spinal nerve pattern of the lumbar region. Comparison of the lumbar nerve pattern in a wt (*A*) and *Hoxa-10*$^{-/-}$ (*B*) adult mice. (*A*) Location of the wt T13, L1–L6, and S1 vertebrae, the last thoracic nerve (a), and the first to the sixth lumbar nerves (b–g) are indicated. (*B*) To show that each change in nerve morphology is accompanied by a corresponding change in vertebral identity, the location of the first to sixth lumbar vertebrae are indicated according to their transformed morphology [T13* represents L1 transformed to a wt T13 identity (note the presence of a supernumerary rib, SR); L1*–L5* correspond to wt L2–L6 identities]. In wt, the last thoracic nerve (a) arises between T13 and L1 and consists of two roots (open double-headed arrow), one of which joins a branch of the first lumbar nerve (b). In *Hoxa-10*$^{-/-}$, a nerve with similar morphology and anatomical relationships as the wt last thoracic nerve (a′, double-headed arrow) is found shifted by one segment between T13* and L1* (the dashed line indicates the location of a branch of the a′ nerve that joined the b′ nerve and was cut during dissection). A nerve with intercostal features [supernumerary intercostal nerve (STN)] is found between T13 and T13* (corresponding to wt T13 and L1, respectively). In wt, the first lumbar nerve (b) arises between L1 and L2 and consists of two roots, one of which joins (a) and the other of which yields the genitofemoral nerve (GFN) together with the second lumbar nerve (c). In the mutant, a nerve with similar morphology and anatomical relationships (b′) is found shifted posteriorly by one segment between L1* and L2*. Note that the branching point (curved arrow) of the GFN is more proximal in the mutant than in wt. Similarly in the mutant each of the following nerves (c′, d′, and e′) displays the morphology of its wt counterpart (c, d, and e) so that the mutant lumbar nerve e′ looks like a wt fourth lumbar nerve (e). In wt, the fifth lumbar nerve (f) arises between L5 and L6, and its root joins the third (d) and fourth (e) nerve roots (square bracket). In *Hoxa-10*$^{-/-}$, there is no nerve that morphologically corresponds to f, perhaps because there is no vertebra with wt L6 morphology (the vertebral transformation stops at S1). Only e′ and d′ roots are joined together (square bracket). The next lumbar nerve that arises in the wt between L6 and S1 (g) and arises in the mutant between L5* and S1 (g) appears to have a normal pathway (thick arrows in *A* and *B*). sc, Spinal cord.

cremaster muscle is originated) or to peritoneal cells (from which the vaginal process develops) could not be unequivocally determined at this stage.

Testicular descent consists of two separate phases (6). During the transabdominal phase of migration, the testes move from their original position in the urogenital ridge to the inguinal region, and by birth they have reached the bladder neck. The inguinoscrotal phase (testis migration into the scrotum) occurs in parallel with gubernacular morphological changes and differentiation, elongation of the vaginal process, and eversion of the cremaster muscle. These processes are under the control of androgens, since they can be experimentally inhibited by androgen antagonists. Furthermore, the androgen-insensitive testicular feminization (*Tfm*) mutant mice (which lack androgen receptor) have intraabdominal testes situated at the level of the bladder neck with no eversion of the scrotal sac (ref. 7 and references therein). In this respect, the *Hoxa-10*$^{-/-}$ phenotype resembles that of the *Tfm* mutation. However, an androgen deficiency is unlikely to be the cause of cryptorchidism in *Hoxa-10* mutants because homozygous males are normally virilized. Furthermore, no androgen receptors were detected in the gubernaculum of wt mice (ref. 7 and references therein), making it unlikely to be a direct target tissue. It has been proposed that the GFN, which innervates the cremaster muscle and the gubernaculum, might mediate androgen action on testicular descent (ref. 7 and references therein). That the spinal nucleus of the GFN is sexually dimorphic, being larger in males than in females (ref. 7 and references therein), supports this hypothesis. Resection of the GFN not only prevents testicular descent but also gubernacular differentiation and vaginal process outgrowth (ref. 7 and references therein), indicating that an intact nerve supply is necessary for testicular descent. The GFN originates from the first and second lumbar spinal cord segments (ref. 7 and references therein). In this report, we note that the first and second lumbar nerves appear to be anteriorly transformed in *Hoxa-10*$^{-/-}$ mice, suggesting that cryptorchidism might be due to incorrect specification of GFN motoneurons and/or abnormal target tissue innervation.

The vertebral morphological alterations observed in *Hoxa-10* mutants were not fully penetrant, even in an inbred genetic background. Furthermore, variations in expressivity evidenced by unilateral abnormalities were seen in some *Hoxa-10*$^{-/-}$ mutants (not shown). Thus, other *Hox* genes might stochastically compensate for the *Hoxa-10* loss of function. The presence of additional ribs on mutant L1 indicates an anterior transformation toward a T13 identity. Interestingly, gain-of-function and loss-of-function mutations of the nonparalogue gene *Hoxc-8* result in a similar transformation (8, 11), indicating that L1 specification is very sensitive to variations in homeoprotein dosage. Furthermore, the incomplete anterior transformations observed for the next lumbar vertebrae suggest that other *Hox* genes with overlapping expression domains are partly redundant with *Hoxa-10*.

The rib alterations in *Hoxa-10* mutants can be interpreted as partial posterior homeotic transformations of thoracic vertebrae. Coexistence of anterior and posterior transformations has been described for other *Hox* gene knock-outs (12, 13).

Since the anterior boundary of *Hoxa-10* expression maps at the level of T13–L1 (data not shown), the mutant thoracic changes between T6 and T12 were not expected. In this respect, we note that knock-outs of the *Hoxa-11* and *Hoxa-6* genes also resulted in vertebral changes outside their normal expression domains (13, 14). One possible explanation is that the integration of a targeting *neo* construct in a *Hox* gene locus might affect the regulation of neighbor genes. The insertion of a PGK-*neo* gene in the homeobox of *Hoxd-10* (a *Hoxa-10* paralogue) resulted in an alteration of the expression domain of the neighbor gene *Hoxd-9* (9). Our *in situ* analysis showed normal expression domains for both *Hoxa-11* and *Hoxa-9* in heterozygous and homozygous *Hoxa-10* mutants. Interestingly, the *neo* gene of the targeting construct PGK-*neo* exhibited a specific *Hox*-like expression pattern extending more rostrally than that of *Hoxa-10*, and overlapping that of *Hoxa-9*. Thus, upon targeted integration, the phosphoglycerate kinase promoter may respond to regulations that control *Hoxa-9* expression, and the corresponding transcription might alter the normal transcript levels of the neighbor *Hoxa-9* gene.

One interesting finding in the present study is that the *Hoxa-10*$^{-/-}$ mice display homeotic transformations of spinal nerves in the lumbar region between T13 and L6. Each nerve adopts, in the mutant, the morphological appearance of the closest rostral wt nerve. This change parallels the vertebral anterior transformations in the same region. Since the segmental pattern of the spinal nerves is governed by the adjacent somite mesoderm (the spinal cord is not intrinsically segmented) (15), it is possible that the vertebral identity might also impose the morphological identity of the associated peripheral nerve. In the lumbar region of the *Hoxa-10*$^{-/-}$ mutants, the spinal neuron pools giving rise to each nerve would then project their axons one segment more posteriorly than in the wt mice. Alternatively, the morphological changes observed in the *Hoxa-10*$^{-/-}$ mutants might reflect actual changes in the positional identities of several components of each lumbar "metameric" unit so that the identities not only of vertebrae but also of spinal neurons and their muscle cell targets would be changed. We favor the latter interpretation for the following considerations: (*i*) in the *Hoxa-10*$^{-/-}$ mice, an intercostal nerve (STN, Fig. 4*B*) is present between T13 and T13* in place of a wt last thoracic nerve; since the number of presacral nerves and vertebrae is the same in mutant and wt mice, it is likely that this nerve derives from the same pool of spinal neurons that would give rise in the wt mouse to a last thoracic nerve; and (*ii*) in the *Hoxa-10*$^{-/-}$ mice, the morphological appearance of the entire region between T13 and T13* is reminiscent of the region between T12 and T13. This is evident from the presence not only of an extra rib on T13* and of the STN but also of muscles in the interrib space resembling intercostal muscles and of an artery resembling an intercostal artery (Fig. 4*B*). Altogether, these results strongly suggest that in the lumbar region of the *Hoxa-10* mutants, several segmented (somite derivates) and nonsegmented (spinal cord derivatives) structures have been homeotically transformed toward more rostral identities. Interestingly, transplantation experiments (16) have postulated the existence of rostrocaudal positional labels shared by nerve and muscle that are involved in the selectivity of target recognition. Our results suggest that the *Hox* genes could provide the positional cues shared by neurons and their targets for the specification of neural connectivity among positionally matched partners.

We thank M. LeMeur and the mouse facility staff; V. Fraulob and M. Poulet for excellent technical assistance; and R. Taneja, A. Gavalas, and M. Davenne for discussion. This work was supported by grants from the Institute National de la Santé et de la Recherche Médicale, the Centre National de la Recherche Scientifique, the Centre Hospitalier Universitaire Régional, the Association pour la Recherche sur le Cancer, the Human Frontier Science Program, and the Fondation pour la Recherche Médicale. F.M.R. was supported by a fellowship from the Association pour la Recherche sur le Cancer.

1. Krumlauf, R. (1994) *Cell* **78,** 191–201.
2. Dollé, P. & Duboule, D. (1989) *EMBO J.* **8,** 1507–1515.
3. Haack, H. & Gruss, P. (1993) *Dev. Biol.* **157,** 410–422.
4. Adra, C. N., Boer, P. H. & McBurney, M. W. (1987) *Gene* **60,** 65–74.
5. Rijli, F. M., Mark, M., Lakkaraju, S., Dierich, A., Dollé, P. & Chambon, P. (1993) *Cell* **75,** 1333–1349.
6. Wensing, C. J. G. (1988) *Horm. Res.* **30,** 144–152.
7. Hutson, J. M. & Beasley, S. W. (1988) *Semin. Urol.* **2,** 68–73.
8. Pollock, R. A., Jay, G. & Bieberich, C. J. (1992) *Cell* **71,** 911–923.
9. Rijli, F. M., Dollé, P., Fraulob, V., LeMeur, M. & Chambon, P. (1994) *Dev. Dyn.* **201,** 366–377.
10. Satokata, I., Benson, G. & Maas, R. (1995) *Nature (London)* **374,** 460–463.
11. Le Mouellic, H., Lallemand, Y. & Brulet, P. (1992) *Cell* **69,** 251–264.
12. Horan, G. S. B., Wu, K., Wolgemuth, D. J. & Behringer, R. R. (1994) *Proc. Natl. Acad. Sci. USA* **91,** 12644–12648.
13. Small, K. M. & Potter, S. S. (1993) *Genes Dev.* **7,** 2318–2328.
14. Kostic, D. & Capecchi, M. R. (1994) *Mech. Dev.* **46,** 231–247.
15. Lim, T., Jaques, K. F., Stern, C. D. & Keynes, R. J. (1991) *Development (Cambridge, U.K.)* **113,** 227–238.
16. Wigston, D. J. & Sanes, J. R. (1985) *J. Neurosci.* **5,** 1208–1221.